ANL/TD/CP-86631
CONF-950905--7

# Activation Analysis for ITER Design Options*



Hosny Attaya
Argonne National Laboratory
9700 South Cass Avenue
Argonne, Illinois 60439 USA



September 1995

*Work supported by the U.S. Department of Energy, Office of Fusion Energy, under Contract No. W-31-109-Eng-38.

To be presented at the 16th Symposium on Fusion Engineering, September 30 - October 5, 1995, Champaign, Illinois.

## DISCLAIMER

Portions of this document may be illegible electronic image products. Images are produced from the best available original document.

# Activation Analysis for ITER Design Options*

Hosny Attaya
Argonne National Laboratory
9700 S. Cass Ave, Bldg 207, Argonne, Il 60439

## ABSTRACT

This paper presents a summary of the activation analyses that have been performed for the shielding blanket (SS/water) and for the breeding blanket (Li/V) of ITER design options. The activation code RACC-P, which has been modified for pulsed operation, has been used in these calculations. The spatial distributions of the radioactive inventory, decay heat, biological hazard potential, and the contact dose were calculated for the two designs for different operation modes and targeted fluences. A one-dimensional toroidal cylindrical geometrical model has been utilized to determine the neutron fluxes in the two designs. The results are normalized for an inboard and outboard neutron wall loadings of 0.91 and 1.2 $MW/m^2$, respectively.

## INTRODUCTION

The objective of the International Thermonuclear Experimental Reactor (ITER) is to demonstrate the scientific and technologic feasibility of fusion energy for peaceful purpose. As the ITER's Engineering Design Activities (EDA) phase evolves, guided by this objective, detailed calculations of the radioactive inventory, dose, and decay heat of the design(s) are required to assess the integrity, the safety aspects, the accessibility, and the waste management of the machine and its different parts that are subjected to neutrons interaction. These different characteristics depend on the choice of the materials and the operation scenario of ITER.

At this stage of the EDA, ITER operation is envisioned into two phases. The first phase, the Basic Performance Phase (BPP), is devoted to physics issues and testing of blanket modules and will include thousands of hours of full DT operation in about ten years. The second phase, the Enhanced Performance Phase (EPP), will focus on improving overall performance and carrying out a higher fluence component and material testing programs and may address reactor-relevant blanket segment demonstration. This phase will accumulate a fluence of at least 1 $MWa/m^2$ and up to 3 $MWa/m^2$ in about ten years. The DT operation in the first phase will depend on the availability of external tritium supply. Provisions are made to breed tritium during the EPP. As a result, the BPP has only shielding blanket which is made of stainless steel/water. In the EPP a ceramic breeder, $Li_2O$ or $Li_2ZrO_3$, with beryllium neutron multiplier and water coolant is being proposed for compatibility with the shielding blanket. However, earlier in the EDA, an advanced blanket design concept using self-cooled liquid lithium and vanadium structure was considered for ITER.

In this paper, we summarize the activation calculations made for the BPP's shielding blanket design [1] and the earlier lithium-vanadium blanket design [2]. Detailed information and results can be found in References 1 and 2. The activation code RACC-P [3], which includes accurate treatment of pulsed operation [4], has been used in these calculations together with the transport code ONEDANT [5].

## THE SHIELDING BLANKET

A one-dimensional toroidal cylindrical geometrical model has been used to represent the inboard and the outboard blanket-shield and vacuum vessel assemblies to account for the toroidal effects of the plasma neutron source. The midplane radial build of the design used in this model is given in Table 1. It should be noted that this design is not as recent as the current ITER design.

The blanket-shield is about 54 cm-thick and consists of a 0.8 cm Be coating, 0.5 cm copper first wall assembly followed by alternating layers of Stainless-Steel 316 (SS) and water as a coolant. The vacuum vessel (VV) is 40.5 cm-thick in the inboard and 56.9 cm-thick in the outboard. The VV structural material is made of the Inconel 625 alloy and has 60:40 mixture of SS:water (SS_H2O) used as a shield. A 5.0 cm-thick boron carbide/lead layer (B4C_Pb) follows the VV to enhance the gamma and the neutron attenuation just before the toroidal field magnet. The results presented here are normalized for an inboard and an outboard neutron wall loadings of 0.91 and 1.2 $MW/m^2$, respectively.

Fig. 1 shows a schematic of the midplane radial build-up together with the neutron and photon fluxes. In this figure, for illustrative purposes and in order to show the characteristics of these fluxes and the effects of the different materials on them, all the photon groups are collapsed into only one group, and the neutron groups are collapsed into 5 major energy groups whose lower energy limits are 10 MeV, 1 MeV, 0.12 MeV, 0.87 eV, and $10^{-4}$ eV. The neutron attenuation in the SS and the absorption in water and boron are clear.

* This work was supported by Office of Fusion Energy, DOE contract No. w-31-109-ENG-38.

Table 1. The radial build of the SS/Water design.

| Z # | dr | Mix | R1 | R2 |
|---|---|---|---|---|
| | cm | | cm | cm |
| | 287.5 | vac | 0.0 | 287.5 |
| 1 | 89.4 | coil | 287.5 | 376.9 |
| 2 | 0.1 | INSUL | 376.9 | 377.0 |
| | 13.5 | vac | 377.0 | 390.5 |
| 3 | 5.0 | B4C_Pb | 390.5 | 395.5 |
| 4 | 5.0 | VV-incl | 395.5 | 400.5 |
| 5 | 30.5 | SS_H2O | 400.5 | 431.0 |
| 6 | 5.0 | VV-incl | 431.0 | 436.0 |
| | 5.0 | vac | 436.0 | 441.0 |
| 7 | 6.9 | SS | 441.0 | 447.9 |
| 8 | 3.1 | H2O | 447.9 | 451.0 |
| 9 | 4.2 | SS | 451.0 | 455.2 |
| 10 | 3.0 | H2O | 455.2 | 458.2 |
| 11 | 7.0 | SS | 458.2 | 465.2 |
| 12 | 3.0 | H2O | 465.2 | 468.2 |
| 13 | 5.5 | SS | 468.2 | 473.7 |
| 14 | 3.0 | H2O | 473.7 | 476.7 |
| 15 | 5.0 | SS | 476.7 | 481.7 |
| 16 | 3.0 | H2O | 481.7 | 484.7 |
| 17 | 2.3 | SS | 484.7 | 487.0 |
| 18 | 2.0 | H2O | 487.0 | 489.0 |
| 19 | 1.0 | SS | 489.0 | 490.0 |
| 20 | 3.6 | H2O | 490.0 | 493.6 |
| 21 | 0.1 | SS(FW) | 493.6 | 493.7 |
| 22 | 0.5 | Cua | 493.7 | 494.2 |
| 23 | 0.8 | BeZ | 494.2 | 495.0 |
| | 11.6 | vac | 495.0 | 506.6 |
| | 608.4 | source | 506.6 | 1115.0 |
| | 16.3 | vac | 1115.0 | 1131.3 |
| 24 | 0.8 | BeZ | 1131.3 | 1132.1 |
| 25 | 0.5 | Cua | 1132.1 | 1132.6 |
| 26 | 0.1 | SS(FW) | 1132.6 | 1132.7 |
| 27 | 3.6 | H2O | 1132.7 | 1136.3 |
| 28 | 1.0 | SS | 1136.3 | 1137.3 |
| 29 | 2.0 | H2O | 1137.3 | 1139.3 |
| 30 | 2.3 | SS | 1139.3 | 1141.6 |
| 31 | 3.0 | H2O | 1141.6 | 1144.6 |
| 32 | 5.0 | SS | 1144.6 | 1149.6 |
| 33 | 3.0 | H2O | 1149.6 | 1152.6 |
| 34 | 5.5 | SS | 1152.6 | 1158.1 |
| 35 | 3.0 | H2O | 1158.1 | 1161.1 |
| 36 | 7.0 | SS | 1161.1 | 1168.1 |
| 37 | 3.0 | H2O | 1168.1 | 1171.1 |
| 38 | 4.2 | SS | 1171.1 | 1175.3 |
| 39 | 3.1 | H2O | 1175.3 | 1178.4 |
| 40 | 6.9 | SS | 1178.4 | 1185.3 |
| | 37.5 | vac | 1185.3 | 1222.8 |
| 41 | 5.0 | VV-incl | 1222.8 | 1227.8 |
| 42 | 46.9 | SS_H2O | 1227.8 | 1274.7 |
| 43 | 5.0 | VV-incl | 1274.7 | 1279.7 |
| 44 | 5.0 | B4C_Pb | 1279.7 | 1284.7 |
| | 15.3 | vac | 1284.7 | 1300.0 |
| 45 | 0.1 | INSUL | 1300.0 | 1300.1 |
| 46 | 89.4 | coil | 1300.1 | 1389.5 |

## A. *Radioactivity and BHP$_{air}$*

Fig. 2 shows the radioactivity per one cm height in this design after operating up to a neutron fluence of 3 MWa/m$^2$. There is about 8 MCi/cm of radioactivity after the shutdown. The isotopic contributions to this activity are shown in the top part of the figure and the zonal contributions (see Table 1) are shown in the bottom part. In this figure only isotopes or zones that contribute more than 10% to the total response, at any time, are shown. The shadowed area at the top represents the contributions of all other isotopes or zones not shown in the figure.

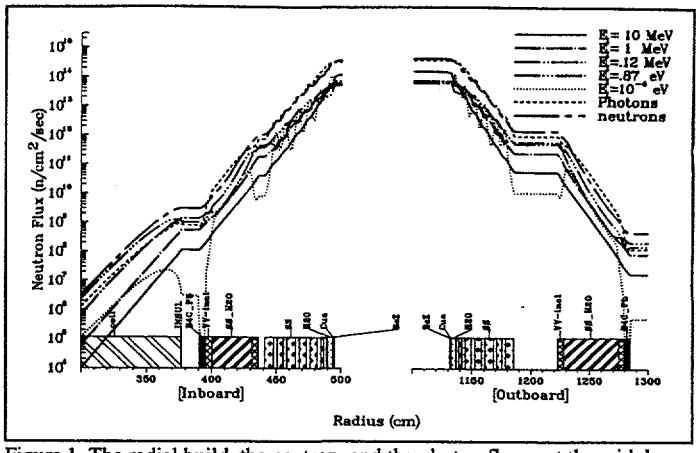


Figure 1. The radial build, the neutron, and the photon fluxes at the midplane.

The FW 0.5 cm Cu layers (zones 22 and 25) produce more than 40% of the total radioactivity in the design after shutdown and for about one day. It dominates the radioactivity also at about 100 years after shutdown, since it yields a large fraction of the $^{63}$Ni ($T½$=100 y, β–) isotope in the system. The outboard SS shield zones (30, 32, and 28) have more than half of the radioactive inventory in the system after about one day after shutdown and for about ten years. The dominant isotope in this period is $^{55}$Fe ($T½$=2.73 y, *EC*). These zones dominate the radioactive inventory again after few hundreds years due to the production of $^{59}$Ni ($T½$=75000 y, EC). These zones remain the longest active zones together with the beryllium zones (24 and 23) because of the production of $^{53}$Mn, and $^{10}$Be isotopes which have long lifetimes.

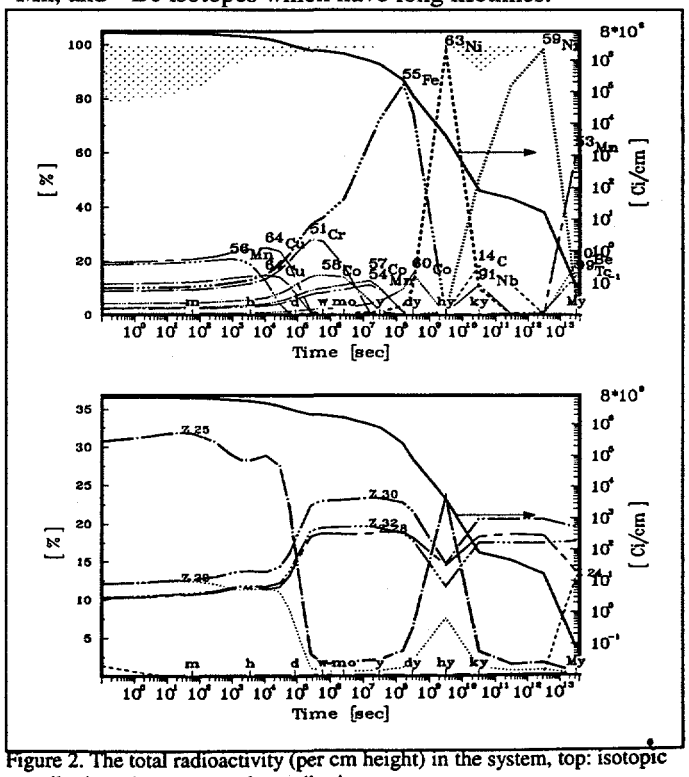


Figure 2. The total radioactivity (per cm height) in the system, top: isotopic contributions; bottom: zonal contributions.

The $BHP_{air}$ of the reactor (not shown) is dominated by the SS zones except in the very short time after shutdown, where it is dominated by the Be zones because of the production of $^{8}Li$ and $^{6}He$.

B. *Decay Heat*

At shutdown, and after 3 MWa/m$^2$ neutron fluence, there is about 50 kW/cm of radiation power. Fig. 3 shows the decay heat (right axis), the isotopic contribution (top-left axis), and the zonal contribution (bottom-left axis). The isotopes $^{56}Mn$ ($T½$=2.6 h, β–, 1.7 MeV $\tilde{\gamma}$ ), $^{16}N$ ($T½$=7 s, β–, 7 MeV γ), $^{64}Cu$ ($T½$=12.7 h, EC-β–), and $^{62}Cu$ ($T½$=9.7 min, *EC*) dominate the afterheat after shutdown and for about one day. For a few years afterward, the isotopes $^{58}Co$ ($T½$=71 d, *EC*, .8 MeV$\tilde{\gamma}$ ) $^{54}Mn$ ($T½$=312 d, *EC*, .8 MeV$\tilde{\gamma}$ ) and $^{60}Co$ ($T½$=5.3 y, β–,2.5 MeV$\tilde{\gamma}$ ) generate most of the decay heat.

It is interesting to notice that about 60 to 90% of this power is produced by photons. This is significant since in the LOCA analyses [6,7] the decay heat is assumed localized where it is produced. This leads to a large concentration of heat that in turn produces hot spots. The fact that a large fraction of this heat is generated by photons, which have a larger range than the charged particles, may level the heat concentration throughout the system thus relieving the energy concentration at high intensity source locations such as the first wall. Accurate modeling for the decay gamma transport is required to produce realistic spatial distribution of the decay heat which may be used in LOCA and LOFA analyses.

C. *Contact Dose*

The point-wise distributions of the decay gamma sources have been calculated everywhere in the reactor at several times after the shutdown and are then used in the transport code ONEDANT to calculate the biological dose everywhere in the reactor. The point-wise distributions of all the responses have also been calculated. These calculations have been performed for neutron fluences of 3.0 MWa/m$^2$, which corresponds to the target maximum fluence of ITER, 1.0 MWa/m$^2$, which corresponds to the minimum fluence, and 0.1 MWa/m$^2$, which is anticipated to correspond to the beginning of an extended maintenance period.

Fig. 4 shows the dose distribution after the 0.1 MWa/m$^2$ fluence. As seen, the recommended dose rate limit of 2.5 mrem/hr for a full time worker can not be attained in most of the reactor for a long time after shutdown. The contact dose results for the longer operation fluences are about an order of magnitude higher than that shown in Fig. 4.

D. *Pulsed Operation*

Three operational scenarios were considered to reach the target design fluence of 3 MWa/m$^2$. The first is simply the

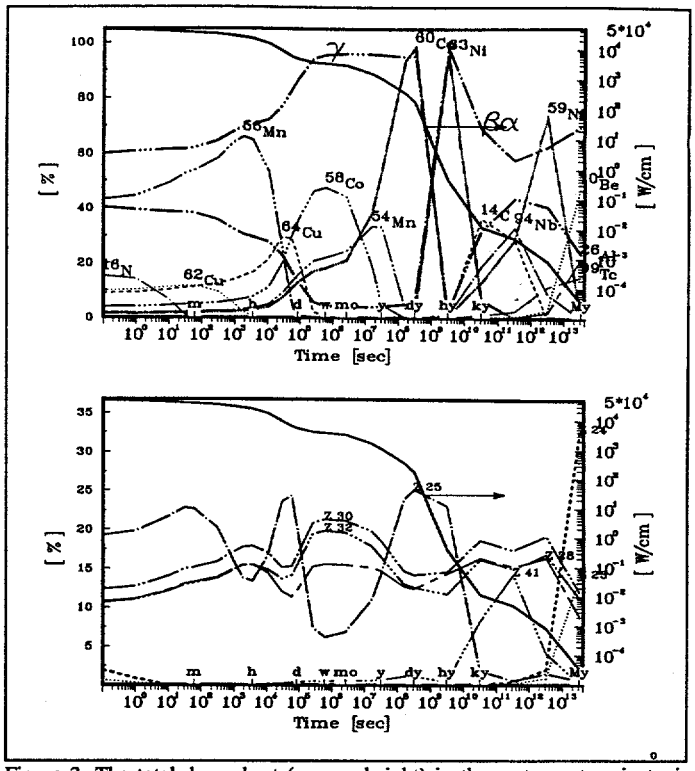


Figure 3. The total decay heat (per cm height) in the system, top: isotopic contributions, bottom: zonal contributions.

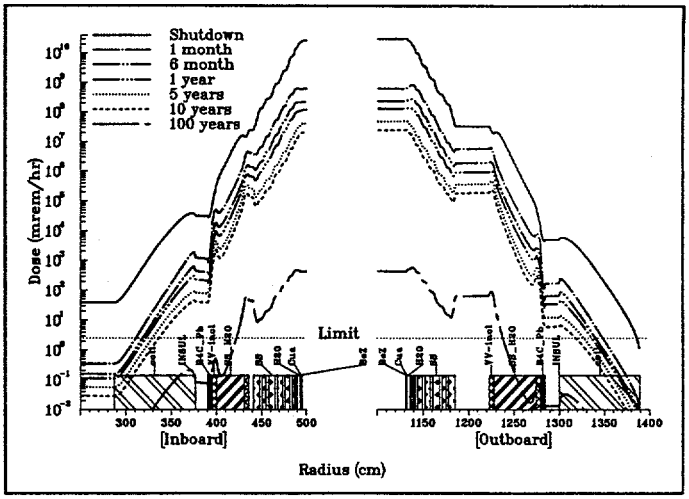


Figure 4. The contact dose distribution at different times after shutdown and after 0.1 MWa/m neutron fluence.

continuous operation mode. Assuming a burn time and dwell time of 1000 and 2039 seconds, the second scenario assumes 103652 cycles. The third scenario consists of 101777 cycles followed by two weeks of continuous operation. We show the results of these scenarios for the inboard FW, for which a total of 3.25 years of continuous operation is required to reach the target fluence.

The specific activity in the inboard FW for the three operation scenarios are shown in Fig. 5. It is evident that the continuous operation mode overestimates the specific activity, and similarly the decay heat and the dose, at the final shutdown and for about one week after shutdown by about a factor of

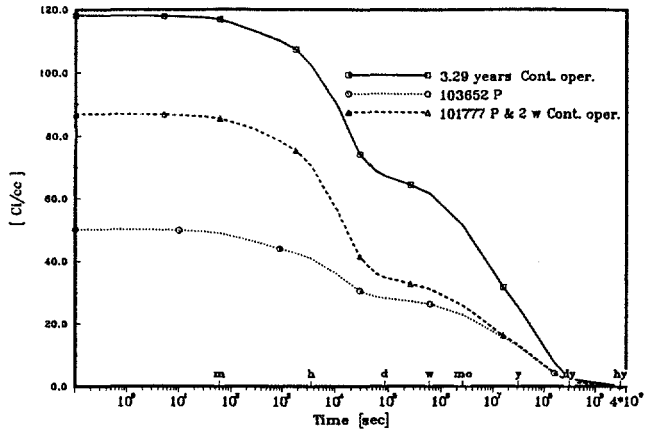


Figure 5. The radioactivity in the inboard SS FW after the three different operation scenarios.

2.4 more than the pure pulse operation mode. Adding a short period of continuous operation (two weeks as in the third scenario) decreases this factor considerably. The difference between the different operation scenarios decreases afterward and vanishes, as expected [8], after a long cooling time.

One expects that for an experimental device such as ITER, there would be longer shut-down periods between pulses and a limited numbers of long burn-time pulses. This would make the radioactivity inventory even less than that of the pure pulsed scenario. Thus, in order to alleviate safety constraints on the ITER design, it is important to have a reasonable estimate of the operation scenario of ITER.

## LITHIUM-VANADIUM DESIGN

This design option was considered at the earlier stage of the DEA. The design utilizes the self-cooled liquid lithium concept for tritium breeding. The vanadium alloy (V-4Cr-5Ti) is used as the structural material because it has several attractive properties including good mechanical and neutron irradiation resistance properties with high heat loads and at high temperatures. It uses beryllium, tungsten carbide, and NaK to enhance the shielding performance. A net TBR of 1.1 has been achieved in this design ensuring a tritium self-sufficiency for ITER operation.

Detailed activation calculations have been made also for this design [2] with the same neutron wall loadings and fluences used in the SS shielding design. The tungsten carbide shields of this design dominate all the activation responses for about one year. Afterward and discarding the activity of the lithium zones, the VV dominates all the activation responses.

Again, as noticed above, a large fraction of the decay heat in this design is also produced by photons. The contact dose has been calculated everywhere in the design and after different fluences and is shown in Fig. 6 after the 0.1 MWa/m$^2$ neutron fluence. Although the dose in the reactor cavity is slightly less than that observed for the SS design, still the accessibility of the machine is limited for a long time after shutdown.

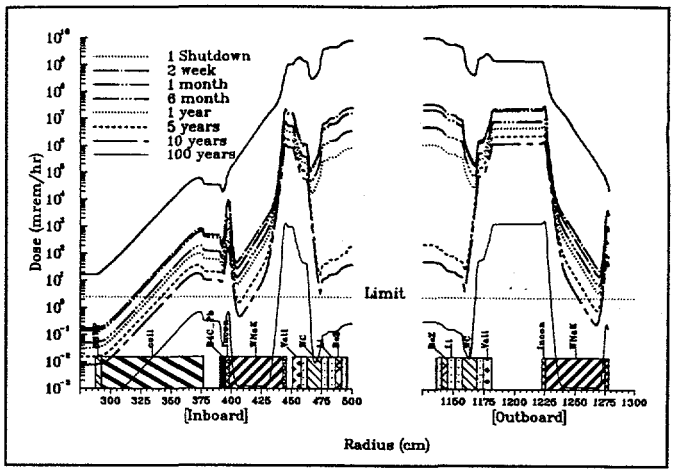


Figure 6. The contact dose distribution in the Li/V design after 0.1 MWa/m$^2$ neutron fluence.

## CONCLUSIONS

Detailed activation analyses have been made for the SS/water and for the lithium-vanadium design options of ITER. The spatial distributions of the different activation responses have been calculated. The decay heat results show that a large fraction of this energy (50 to 90%) is produced by photons. Accurate modeling of the pulsed operation results in a large reduction of the different activation responses. The contact dose results show that most of the machine would not be accessible for a long time after shutdown.

## ACKNOWLEDGMENT

This work was supported by the Office of Fusion Energy, US Dept. of Energy under Contract No. W-31-109-ENG-38.

### References

[1] H. Attaya, "Summary Report for ITER TASK - D4, Activation Calculations for the Stainless Steel ITER Design," Argonne National Laboratory, ANL/FPP/TM-276, ITER/US/IV-BL-16-A, (1995).

[2] H. Attaya, "Summary Report for ITER TASK - D4, Activation Calculations for the Lithium Vanadium ITER Design," Argonne National Laboratory, ANL/FPP/TM-282, ITER/US/IV-BL-16-B, (1995).

[3] H. Attaya, "Input Instructions for RACC-P," Argonne National Laboratory, ANL/FPP/TM-270 (1994).

[4] H. Attaya, "Radioactivity Computation of Steady-State and Pulsed Fusion Reactors Operation," Fus. Eng. and Design 28 (1995) 571.

[5] R.D. O'Dell et al., "User's Manual for ONEDANT: a code package for one-dimensional, diffusion-accelerated neutral particle transport," Los Alamos National Laboratory Report, LA-9184-M (1989).

[6] H. Attaya et al., "Two Dimensional LOCA Analysis for Fusion Reactors," Proc. Of 13th IEEE Symposium on Fusion Engineering, Knoxville, TN, IEEE Cat. No. 89CH2820, 1120 (1989).

[7] H. Attaya, "LOCA Analysis for Manganese-Stabilized Steel," Fusion Technology Vol. 19, 1331 (1991).

[8] H. Attaya et al., "US-ITER Activation Analysis," Fusion Technology Vol. 19, 1837 (1991).